Hover and Forward Flight Performance Modeling of the Ingenuity Mars Helicopter

Cuyler Dull
Aeromechanics Intern
NASA Ames Research Center
Moffett Field, California

Lauren Wagner
Aerospace Engineer
NASA Ames Research Center
Moffett Field, California

Larry Young
Aerospace Engineer
NASA Ames Research Center
Moffett Field, California

Wayne Johnson
Aerospace Engineer
NASA Ames Research Center
Moffett Field, California

ABSTRACT

In 2015, NASA's Jet Propulsion Laboratory partnered with Ames Research Center, Langley Research Center, and AeroVironment to develop Ingenuity, a small coaxial helicopter capable of flying within Mars' unique atmospheric conditions. Ingenuity was successfully deployed from its protective shroud on the underside of the Mars 2020 Perseverance Rover and has flown 17 flights on Mars as of December 2021. A number of rotorcraft analysis tools were utilized, and a series of experimental tests were performed to ready Ingenuity for its launch with the Perseverance Rover in July 2020. In this paper, RotCFD, a Reynolds-averaged Navier-Stokes flow solver, is used to model Ingenuity in hover and forward flight for the purposes of validating tools to aid in the development of a future generation of Mars rotorcraft. The results from the RotCFD modeling are benchmarked against results from hover performance tests of the Ingenuity prototype in the 25-Foot Space Simulator at the Jet Propulsion Laboratory and are also compared to hover and forward flight predictions made by CAMRAD II, a well-known comprehensive rotorcraft analysis code. Surrogate performance models are trained to obtain a set of trimmed rotor settings for Ingenuity at different forward flight speeds, which are then used as inputs for the RotCFD forward flight simulations. Additionally, a study of the airframe-rotor interaction and a study of the aerodynamics of the individual airframe components of Ingenuity in forward flight are performed. Finally, to better understand performance predictions by RotCFD and CAMRAD II, a study is conducted on how sectional angles of attack in each code vary with radial station and azimuth.

NOTATION

A	rotor disk area, m^2
C	Courant number
C_P	power coefficient, $P/(\rho A V_{tip}^3)$
C_T	thrust coefficient, $T/(\rho A V_{tip}^2)$
C_Q	torque coefficient, $Q/(\rho A V_{tip}^2 R)$
D	drag, N
F_{DL}	airframe download, N
g	acceleration due to gravity, m/s^2
H	in-plane rotor drag, N
L	lift, N
m	mass, kg
M	hover figure of merit
M_{tip}	rotor tip Mach number
p	fluid pressure, Pa
P	rotor power, W
q	dynamic pressure, N/m^2
Q	rotor torque, N $\cdot$ m
r	rotor disk radial coordinate, m
r_D	lever arm of drag force, m
R	rotor radius, m

Re	Reynolds number
t	time, s
T	rotor thrust, N; temperature, K or °C
v_{ff}	forward flight speed, m/s
V_{tip}	rotor tip speed, m/s
W	weight, N
X	free-stream axis drag force, N
γ	specific heat ratio
δ_P	differential collective, deg.
θ	rotorcraft pitch attitude (positive values indicate forward tilt)
$\theta_{0.75}$	collective pitch angle at 75% radius
μ	dynamic viscosity, (N $\cdot$ s) / m^2
ρ	density, kg/m^3
σ	rotor solidity

C81Gen	C81 Generator
CAMRAD	Comprehensive Analytical Model of Rotorcraft Aerodynamics and Dynamics
CFD	Computational Fluid Dynamics
DoE	Design of Experiments
JPL SS	Jet Propulsion Laboratory Space Simulator

MC	Mars Condition
RANS	Reynolds-Averaged Navier Stokes
RotCFD	Rotorcraft Computational Fluid Dynamics
RotUNS	Rotor Unstructured Solver

INTRODUCTION

NASA developed the Ingenuity Mars Helicopter to improve upon the range, mobility, and three-dimensional exploration capability of rovers and landers used in previous Mars missions. Rotorcraft on Mars are intended to act as scouts for rovers, improve the resolution of surface images with respect to satellite images, and expedite sample gathering. However, the atmosphere's low density and temperature necessitates rotor operation in uninvestigated Mach-Reynolds number regions [1]. Given Mars' unique atmosphere, extreme terrain, and weak gravitational pull, careful consideration was necessary in the design of this first-generation Martian rotorcraft.

Ingenuity Design:

Ingenuity—shown in Figure 1—has a mass of 1.8 kg and a rotor diameter of 1.21 m. The rotor system consists of two counter-rotating coaxial rotors. This design benefits from a compact rotor system, increased thrust per unit of power with respect to non-coaxial rotor systems, torque balancing from counter-rotating rotors, and symmetry of lift during forward flight. To reduce weight and maintain structural integrity, the blades were built using a molded foam-core composite structure; bi-directional carbon fiber was cured around a machined foam core, yielding blades that weigh only about 28 grams each [2]. Ultralightweight rotors and vehicle hardware is key to the success of Mars rotorcraft.

Figure 1: Ingenuity on the surface of Mars [3]

Above the rotors is a solar array which captures solar energy to charge the battery system. Ingenuity's landing gear consists of four carbon-fiber legs which emanate diagonally from the top of the airframe, offering a large footprint for stable take-off and landing maneuvers. Titanium flexures at the top of each leg offer suspension during landing.

Ingenuity's guidance, navigation, and control is provided by a commercial off-the-shelf inertial measurement unit, laser altimeter, processor and camera, and field-programmable gate array chips [4]. The demonstration of solar-electric rotor propulsion by Ingenuity through periodic battery recharging is a key enabler of sustained multi-Sol and multi-sortie flight missions on Mars for future Mars rotorcraft.

Objective

Just as rotorcraft analysis tools were critical to the development of Ingenuity, the work presented here will support the design and development of future Mars rotorcraft designs. This paper aims to correlate hover and forward flight performance predictions of Ingenuity from a mid-fidelity CFD tool, Rotorcraft CFD (RotCFD), against CAMRAD II, a comprehensive rotorcraft analysis software. Furthermore, these predictions are correlated to experimental hover data acquired in the 25-Foot Jet Propulsion Laboratory Space Simulator (JPL SS). Only recently [5] has an initial set of forward flight test data—using a "wind wall" in the 25-Foot SS been published; correlation with this experimental data, and perhaps flight test data from Mars, ought to be included in future work in this area. Nevertheless, this paper seeks to expand upon the effort to enhance modeling fidelity of rotorcraft in Martian conditions.

Rotorcraft CFD (RotCFD) [6] is selected as the aerodynamic modeling environment for Ingenuity for this paper. The software tool provides a robust aerodynamic modeling environment that can model Ingenuity and accurately relate rotorcraft design inputs to performance predictions. RotCFD is a mid-fidelity computational fluid dynamics tool developed by Sukra Helitek—partly under NASA Small Business Innovation Research funding—that uses two-dimensional airfoil data and a Reynolds Averaged Navier Stokes (RANS) solver to simulate unsteady, incompressible flows. RotCFD was one of the tools used during the Ingenuity development, especially in examining test facility interference effects on rotor performance and flight dynamics.

RotCFD is used here to model Ingenuity's coaxial rotors without its airframe in the hover flight condition and Ingenuity's rotors with its airframe in forward flight. For hover simulations, the interrelation between the power and thrust of the rotor is predicted as well as the rotors' figure of merit. For forward flight, the interrelation between the coefficients of thrust and power and forward flight speed is predicted.

Mars Conditions

The atmosphere of Mars consists of approximately 95% carbon dioxide, 2.7% nitrogen, and 1.6% argon [7] with an atmospheric density of approximately 0.017 kg/m^3—about 1.5% of the air density at sea level on Earth [8]. The atmospheric composition and low air temperatures yield a lower speed of sound than Earth's. Furthermore, Ingenuity's small rotor system and the low air density result in low chord-based Reynolds numbers. Together, these factors constrain rotor design and operation, making it more difficult to generate thrust. However, Mars' gravitational acceleration is approximately 3.71 m/s^2—roughly 38% of Earth's—which lowers thrust requirements.

MODELING, SIMULATION, AND TESTING ENVIRONMENTS

NASA Ames Research Center has long had a research interest in the development of Mars rotorcraft, stemming from the late 1990s [9]. Ames' contributions to Ingenuity development included providing expertise and performing engineering tasks for both vehicle analysis and experimental testing. The Ingenuity initial concept was documented in [10] by JPL.

Ingenuity Airfoil Analysis
In 2018, Koning et. al. [8] generated a set of two-dimensional airfoil tables for Ingenuity's blades, which were designed by AeroVironment, Inc. These airfoil aerodynamic coefficient tables were produced by the C81 Generator (C81Gen) software tool, which used the NASA-developed time-dependent compressible RANS solver ARC2D, with the outer software framework developed by Sukra Helitek. Koning et. al. [1] then improved upon this analysis with higher-fidelity, time-accurate simulations in OVERFLOW, an implicit compressible RANS solver [11]. The purpose of the second iteration was to enable higher-accuracy aerodynamic coefficients, a thorough understanding of the flow structure, denser grid meshes, and modeling of realistic trailing edge thicknesses. Airfoil tables were made for both a set of average Martian atmospheric conditions—Mars condition (MC) 2—and JPL SS conditions (see Table 1). MC 1, MC 2, and MC 3 are sets of air properties that represent the low, middle, and high values, respectively, of air density recorded diurnally at the Ingenuity landing location on Mars [8].

Table 1: Operating conditions for MC 2 [8]

Variable	MC 2	JPL SS
Density, ρ [kg/m^3]	0.017	0.0175
Temperature, T [K]	223.15	293.15
Gas constant, R [m^2/(s$^2 \cdot$ K)]	188.90	188.90
Specific heat ratio, γ	1.289	1.289
Dynamic viscosity, μ [(N $\cdot$ s)/m^2]	1.13e-05	1.504e-05
Static pressure, p [kPa]	0.716	0.969
Speed of sound, a [m/s]	233.13	269.44

RotCFD
RotCFD [6] aids with fluid dynamics analysis of rotorcraft, propellers, and wind turbines. RotCFD provides an integrated development environment with an embedded graphical user interface which affords efficient geometry manipulation, grid-generation, pre-processing, flow solving, post-processing, and flow visualization.

The software includes flexible modeling capabilities, both in regard to body geometry manipulation and rotor system representation. RotCFD can model rotors using the unsteady, time-dependent blade element theory or steady, time-independent actuator-disk model. To reduce computational complexity, steady modeling is chosen for these analyses.

To model the aerodynamic performance of Ingenuity, the Rotor Unstructured Solver (RotUNS) is used. This solver operates on an unstructured mesh grid, utilizing three dimensional, incompressible RANS equations to model the flow.

CAMRAD II
Comprehensive Analytical Model of Rotorcraft Aerodynamics and Dynamics (CAMRAD II) is a comprehensive rotorcraft analysis software tool that aids in the design, analysis, and aeromechanics evaluation of rotors and rotorcraft [12]. It provides the ability to predict rotor performance, loads, vibration, and dynamic stability assessments; furthermore, the tool is able to perform trim, transient, and aeroelastic blade flutter tasks.

CAMRAD II models aerodynamic characteristics of rotors using lifting-line theory and free-wake modeling. Two-dimensional airfoil characteristics at various radial rotor stations are prescribed through C81 airfoil input files which, in turn, are computationally used to determine the circulation distribution of each blade and, thus, the flow through the rotor. The free-wake vortex wake is modeled through a combination of rolled-up trailed vortices and inboard vortex sheets.

CAMRAD II has been extensively and successfully used by the rotorcraft design and analysis community in modeling the performance and loads of many types of rotorcraft—including coaxial helicopter configurations [13].

This software is used to model Ingenuity as a set of coaxial rotors in both JPL SS conditions as well as MC 2 conditions in hover, as shown in Table 1. Additionally, CAMRAD II is used to model Ingenuity in a parametric sweep of forward flight speeds to obtain rotor trim settings and forward flight performance predictions. Results from these simulations serve as a benchmark against which RotCFD predictions are compared.

Jet Propulsion Laboratory Space Simulator
The NASA JPL SS is a 25-foot diameter chamber designed to test spacecraft or rotorcraft in simulated interplanetary or Martian conditions. The chamber is able to simulate extreme temperatures, atmospheric densities, and solar radiation levels [14].

To simulate Mars conditions for flight tests, the chamber was evacuated and then backfilled with CO_2 to achieve a density of $\rho = 0.0175$ kg/m^3. Nevertheless, the temperature of the chamber was left at its ambient level of $T = 20°C$.

For hover testing, a full-scale prototype was developed. The prototype's rotor speed was fixed at 2,600 RPM; thus, for the 1.21 m diameter rotor, the tip speed was 165 m/s, or $M_{tip} = 0.62$. To simulate the reduced gravitational pull on

Mars with respect to Earth's, certain elements of the rotorcraft were removed to reduce weight, such as the power source for prototype hover testing. Rather, power was fed to the prototype via an electrical tether.

Nevertheless, the thrust and power consumption measurements from within the JPL SS—the measurements against which RotCFD and CAMRAD II performance predictions are compared in this paper—were captured using a stationary test stand on which Ingenuity's two counter-rotating rotors were mounted. Further information about the JPL SS and the Ingenuity tests are discussed by Balaram and Tokumaru [10].

The results from these JPL experimental tests provide the set of data against which hover performance predictions in RotCFD are compared.

TECHNICAL APPROACH

Hover
A series of CFD simulations is conducted to compare Ingenuity's hover performance predictions in RotCFD against data from the JPL SS and CAMRAD II. Initially, a collective pitch sweep is performed for an isolated rotor to understand the interrelation between a single rotor's collective pitch, thrust, power, and figure of merit.

Once the isolated rotor model is calibrated in RotCFD, a collective pitch sweep is conducted for both rotors configured in their coaxial configuration without the airframe for the same purpose. The airframe is omitted to simplify grid generation and aid in solution convergence.

A key challenge in the control and stability of coaxial counter-rotating rotors is directional stability. To better understand the mode of directional control, a study of differential collective pitch between the rotors is performed. The collective pitch of the top rotor is decreased while the collective pitch of the bottom rotor is increased the same amount about a fixed nominal value. This actuation is known as antisymmetric collective [15]. In effect, the net thrust is nearly held constant while the net yawing moment is varied. A linear model is then fit to quantify the relationship between differential collective setting and the resultant net torque coefficient.

A collective sweep is first performed in MC 2 conditions in RotCFD and CAMRAD II. Then, a collective sweep is performed in JPL SS conditions with both codes. The results from the latter are compared against experimental results from hover tests in the JPL SS in the section titled "Hover Comparison in JPL SS Conditions."

Forward Flight Modeling
For the forward flight condition, RotCFD performance data is compared against CAMRAD II predictions. To model a valid steady-state forward flight condition, all forces and moments need to be balanced. In this paper, the x^+ -axis of

the coordinate system points into the free-stream direction while the z^+ -axis points upward, orthogonal to the free-stream axis. Furthermore, a positive pitch attitude, θ, indicates a forward tilt. This convention is depicted in Figure 2 below.
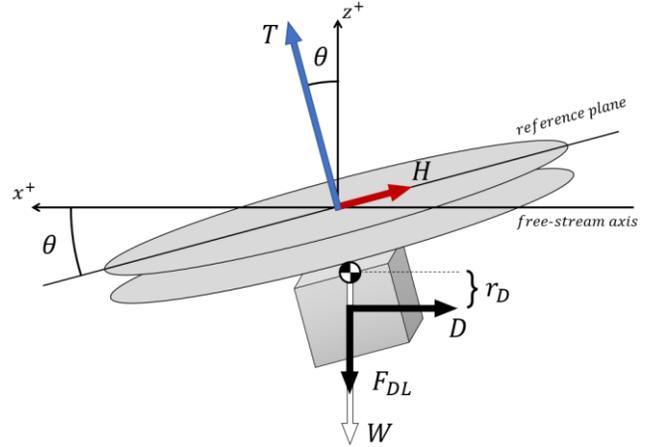

Figure 2: Forward flight coordinate system convention

The z-component of the net rotor thrust and in-rotor-plane drag need to balance with weight, W, and the aerodynamic download on the airframe, F_{DL}.

$$\sum F_Z = T \cdot \cos(\theta) + H \cdot \sin(\theta) - W - F_{DL} = 0 \quad (1)$$

Similarly, the x-component of the net rotor thrust needs to balance the airframe drag, D, and the x-component of the in-rotor-plane drag.

$$\sum F_X = T \cdot \sin(\theta) - H \cdot \cos(\theta) - D = 0 \quad (2)$$

Furthermore, for directional stability, the net rotor torque between the rotors needs to be equal to zero.

$$\sum M_Z = Q_{top} + Q_{bottom} = 0 \quad (3)$$

Longitudinal equilibrium is enforced by balancing the sum of pitching moments of the rotors about Ingenuity's center of gravity and the cross product of the airframe drag and the distance to Ingenuity's center of gravity.

$$\sum M_Y = M_{Y,top} + M_{Y,bottom} - r_D \times D = 0 \quad (4)$$

For simplicity, lateral—or roll—stability is omitted from this analysis. Accordingly, the sensitivity of lateral cyclic pitch is not explored.

In addition, the forces on the airframe will be shown in a set of results. These results will follow the coordinate system set forth here, with drag in the negative x-direction and download in the negative z-direction.

Surrogate Modeling of Rotor Trim Settings for Forward Flight
A surrogate model is constructed to map a given forward flight speed to pitch attitude and a set of trimmed rotor collective settings that yield balanced forces and moments for Ingenuity in level, unaccelerated flight in RotCFD. In contrast, the trim task is leveraged in CAMRAD II to

converge upon trimmed pitch attitude and rotor settings for each forward flight speed.

To begin, a full-factorial design of experiments (DoE) is constructed that sweeps through forward flight speeds, v_{ff}, of 5, 10, 15, 20, 25, and 30 m/s and a range of pitch attitude angles, θ. For forward flight speeds of 5 and 10 m/s, the pitch attitudes span 0 to 8 deg. with an interval of 2 deg. For forward flight speeds of 15, 20, 25, and 30 m/s—where greater pitch attitudes are required to generate the propulsive force that counters drag—the upper and lower limits of pitch attitude angles modeled are increased accordingly. In total, the DoE consists of thirty-six cases. Table 2 details this DoE below.

Table 2: Forward Flight DoE

Case Range	Forward Flight Speed [m/s]	Pitch Attitude Range [deg.]
[1, 5]	5	[0, 8]
[6, 10]	10	[0, 8]
[11,15]	15	[2, 10]
[16, 22]	20	[2, 14]
[23, 29]	25	[2, 14]
[30, 36]	30	[9, 14]

For each case, the trim tool within RotCFD is used to find the collective and cyclic rotor settings that generate a force of 6.75 N—or the weight of Ingenuity on Mars—in the z-direction while balancing moments about the y- and z-axes.

Inevitably, there is an imbalance of forces in the freestream direction as the pitch attitude angle is not trimmed to balance forces in the x-direction. Thus, a neural network surrogate model is trained to map the input space—a given forward flight speed; sum of forces in x and z; and net moment about y and z—to the output space—nominal collective pitch, differential collective, and cyclic settings.

Thus, a user may query rotor settings that yield unaccelerated, level forward flight by inputting a forward flight speed and zeros for the force and moment inputs into the neural network.

Once the trimmed settings are obtained from the neural network, a final forward flight sweep is performed using the trimmed rotor settings. The forward flight performance predictions are then benchmarked against those of CAMRAD II for the same forward flight sweep.

HOVER RESULTS

Differential Collective Torque Matching
For three nominal collective settings—5, 10, and 15 deg.—a differential collective sweep is performed from -1 to 0.6 deg. To clarify, a differential collective setting of -0.5 deg. at a nominal collective setting of 10 deg. would set the top and bottom collective pitches to 9.5 and 10.5 deg., respectively.

Figure 3 depicts how the net torque coefficient of the two rotors varies with differential collective setting for each nominal collective setting. The net torque coefficients for each nominal collective value are uniformly shifted such that the net torque coefficient is zero at a differential collective value of 0 deg.
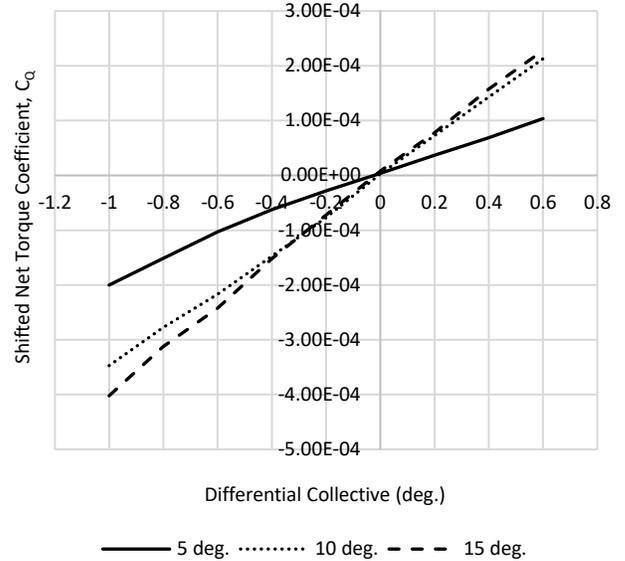

Figure 3: Shifted net torque coefficient versus differential collective for varied collective pitch settings in hover

For each set of data, the partial derivative of net torque coefficient with respect to differential collective setting, $\partial C_Q/\partial \delta_P$, is recorded. The partial derivative for 5, 10, and 15 deg. is calculated as 1.851×10^{-4}, 3.525×10^{-4}, and 3.942×10^{-4} deg.$^{-1}$, respectively. Thus, for the same unit differential collective control input, the change in net torque coefficient increases with nominal collective.

Rotors-Only Hover Comparison in MC 2 Conditions
Hover performance predictions from RotCFD and CAMRAD II are compared for MC 2 conditions. Specifically, a collective sweep is performed for Ingenuity's rotors in their coaxial configuration. For each code, the rotors are trimmed to zero net torque using differential collective.

In Figure 4, the added thrust coefficients of the top and bottom rotors are plotted against collective pitch.
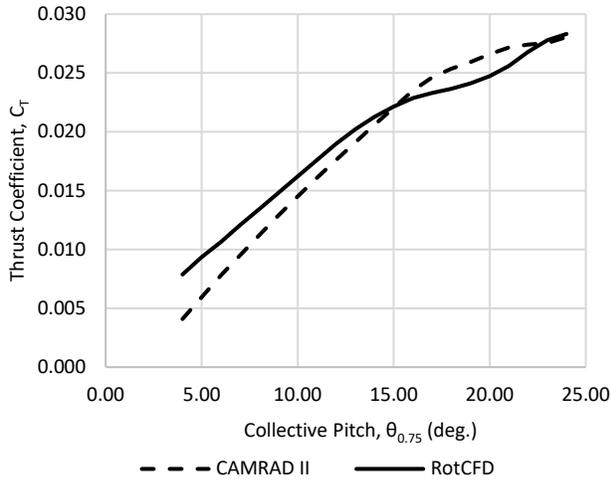
Figure 4: Thrust coefficient versus collective pitch for coaxial rotors in MC 2 conditions

For low collective settings, RotCFD overpredicts thrust coefficients with respect to CAMRAD II. RotCFD and CAMRAD II closely agree for collective settings of 15 and 24 deg., yet RotCFD underpredicts thrust for collective settings between these values.

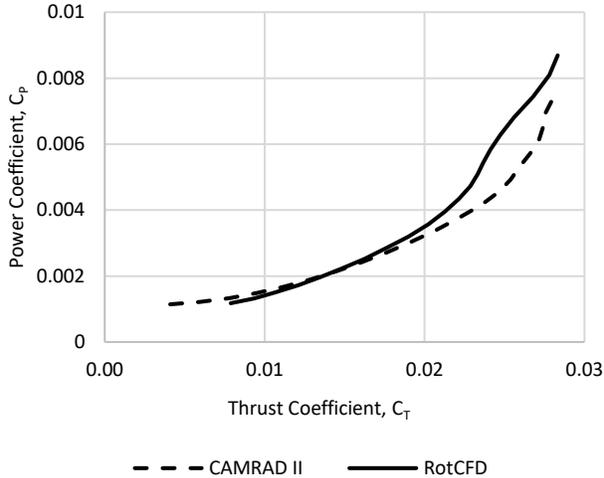Figure 5 depicts how power coefficients vary with thrust coefficients through the collective sweep.

Figure 5: Power coefficient versus thrust coefficient in MC 2 conditions

For the design thrust coefficient range—which spans from thrust coefficients of 0.015 to 0.020 and represents the nominal operation of Ingenuity—there is good agreement between RotCFD and CAMRAD II. For higher thrust settings, RotCFD predicts greater power coefficients.

In Figure 6, the rotors' figure of merit is plotted against thrust coefficient divided by solidity.

Figure 6: Figure of merit versus thrust coefficient over solidity in MC 2 conditions

There is some agreement between the data sets for the design thrust coefficient range. However, for high thrust coefficient settings, there is a divergence in the data sets. RotCFD overpredicts the power coefficient with respect to CAMRAD II; thus, RotCFD underpredicts the rotors' figure of merit for high thrust coefficients with respect to CAMRAD II.

Hover Comparison in JPL SS Conditions
Without the airframe of Ingenuity, the rotors are modeled in their coaxial configuration to elucidate the intra-rotor interaction and total rotor system performance in CAMRAD II and RotCFD. These results are compared against those of the experiments in the JPL SS. Figure 7 below depicts the difference between the coaxial rotors of Ingenuity modeled in RotCFD and the rotors mounted to the thrust-measurement test stand in the JPL SS.

Figure 7: Coaxial rotors of Ingenuity in RotCFD (top) and the thrust-measurement test stand in the JPL SS (bottom) [4]
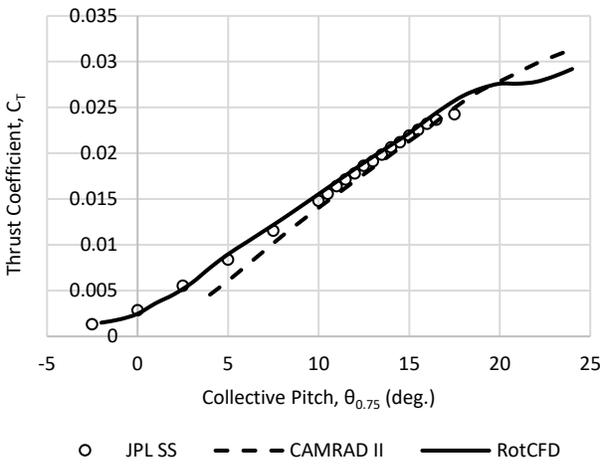
Figure 8: Thrust coefficient versus collective pitch for coaxial rotors in JPL SS conditions

In Figure 8, the thrust coefficients are plotted against collective pitch. The thrust coefficients predicted by RotCFD show satisfactory correlation with those of CAMRAD II and experimental results from JPL SS, particularly for collective pitch settings from 10 to 17 deg.

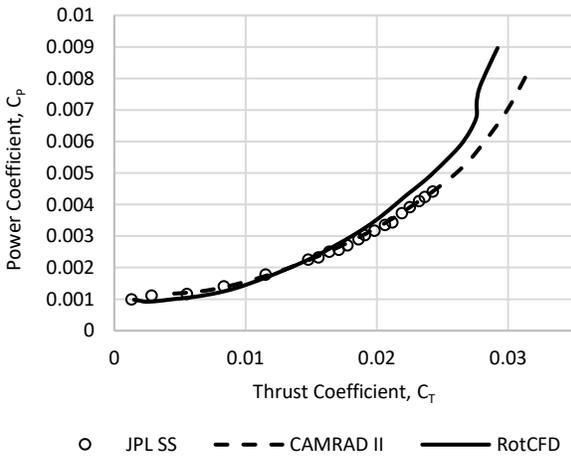Power coefficients are plotted against thrust coefficients in Figure 9.

Figure 9: Power coefficient versus thrust coefficient in JPL SS conditions

As in the case of the MC 2 conditions, there is agreement between the datasets for the design thrust coefficient range. Here, CAMRAD II predictions match the experimental data quite well; though, for higher thrust settings, RotCFD predicts greater power coefficients with respect to the other two datasets.

Figure 10 below depicts the rotors' figure of merit versus thrust coefficient divided by solidity.

Figure 10: Figure of merit versus thrust coefficient over solidity in JPL SS conditions

RotCFD generally agrees with CAMRAD II predictions and experimental results for modest thrust coefficients. However, like the trend observed for MC 2 conditions, RotCFD overpredicts the rotors' power coefficients for high thrust settings with respect to the benchmark data. Thus, a disagreement in the figure of merit trends is observed at these high thrust settings. Nevertheless, CAMRAD II only slightly underpredicts figure of merit with respect to experimental data.

FORWARD FLIGHT RESULTS

Forward Flight Pitch Sweep
The full Ingenuity model—including the coaxial rotors, rotor mast, airframe, legs, and solar array—is included in the forward flight modeling. A forward flight sweep is conducted for forward flight speeds of 5, 10, 15, 20, 25, and 30 m/s.

Figure 11 below depicts a sample velocity vector field for Ingenuity in forward flight at $v_{ff} = 10$ m/s with the freestream entering from the left. From the figure, one can observe the deflection of the flow around the solar array and fuselage and the redirection of freestream flow through the rotor disks.
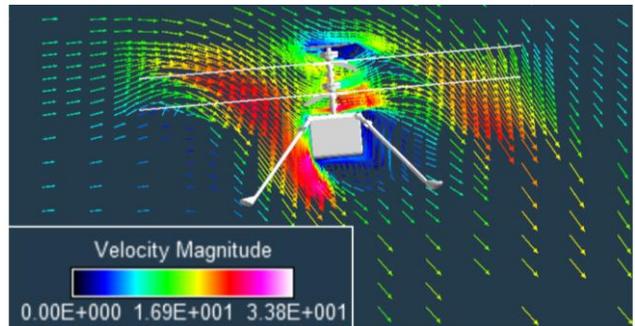

Figure 11: Velocity vector field of Ingenuity in forward flight at 10 m/s [16]

A pitch attitude sweep is performed for each forward flight speed while using a trim tool within RotCFD which balances forces in the z-axis and moments about the y- and z-axes. A linear model is then fit for each forward flight speed between the sum of forces in the x-direction, or freestream-axis, and pitch attitude. These results are depicted below in Figure 12.
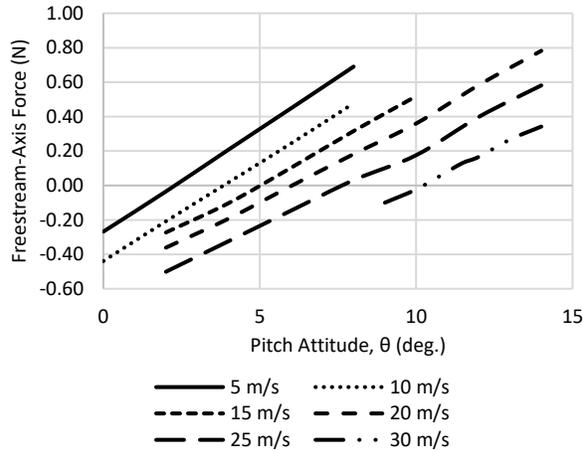

Figure 12: Freestream axis force versus pitch attitude through the forward flight sweep

The x-intercept of each linear model thus represents the pitch attitude for which forces in the free-stream axis are balanced. Figure 13 below illustrates the relationship between trimmed pitch attitude and forward flight speed.

Figure 13: Trimmed pitch attitude versus forward flight speed

There is a monotonic relationship between the forward flight speed and trimmed pitch attitude. As forward flight speed increases so does dynamic pressure and thus airframe drag; furthermore, Ingenuity's hinge-less rotors generate significant pitch moments in forward flight. Consequently, a greater pitch attitude is required to balance freestream forces for higher forward flight speeds.

Trimmed Forward Flight Comparison
Using the trimmed pitch attitudes from the previous section, another forward flight speed sweep is performed. The RotCFD results are plotted against performance predictions

from CAMRAD II. Though, the trimmed model settings—including pitch attitude, collective pitch, differential collective, and cyclic—are independently calculated in each code.

In Figure 14, thrust for each rotor is plotted against forward flight speed.
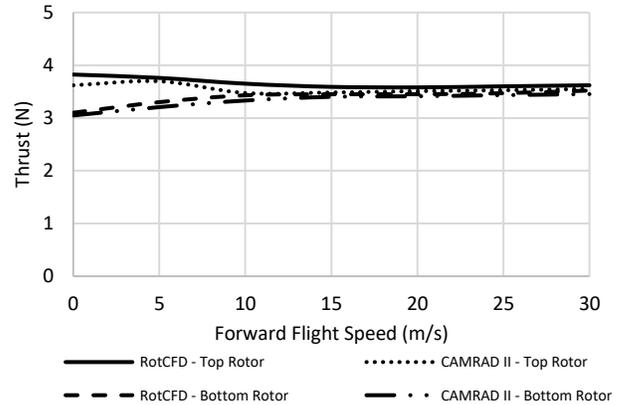

Figure 14: Top and bottom rotor thrust versus forward flight speed

There is a tight correlation between RotCFD and CAMRAD II for the predicted thrust for each forward flight speed. Additionally, both codes predict that the top rotor contributes a greater share of the thrust for low forward flight speeds and that the thrusts approach the same value for higher speeds.

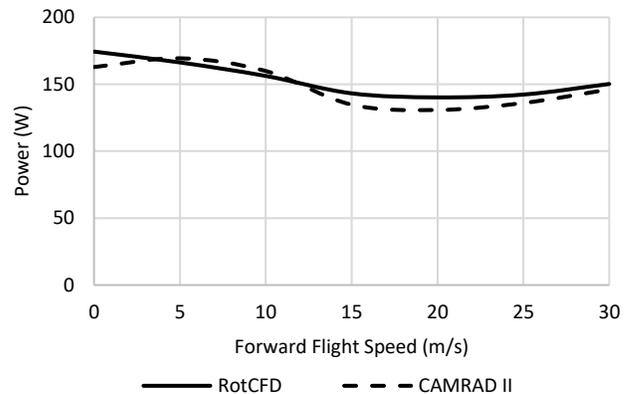Figure 15 plots total rotor power against forward flight speed.

Figure 15: Power versus forward flight speed

Once again, there is general agreement between the two codes; however, the power bucket of CAMRAD II is slightly more pronounced than that of RotCFD. Nevertheless, both codes predict that the lowest power consumption is achieved at a forward flight speed of approximately 18 m/s.

The nominal collective pitch setting is plotted against forward flight speed in Figure 16. Nominal pitch setting is defined here as the average collective pitch of the two rotors.
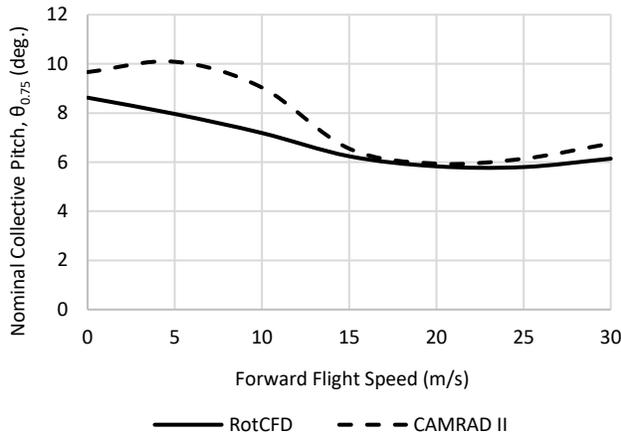

Figure 16: Nominal collective pitch setting versus forward flight speed

For forward flight speeds greater than or equal to 15 m/s, there is a tight correlation between RotCFD and CAMRAD II for the predicted nominal collective pitch setting. However, RotCFD underpredicts the nominal collective pitch setting required from low forward flight speeds with respect to CAMRAD II. In Figure 17, the trimmed differential collective settings are plotted against forward flight speed.

Figure 17: Differential collective setting versus forward flight speed

Like nominal collective pitch setting, there is agreement for the required differential collective for torque matching at high forward flight speeds. However, RotCFD reports lower trimmed differential collective settings than CAMRAD II at low speeds.

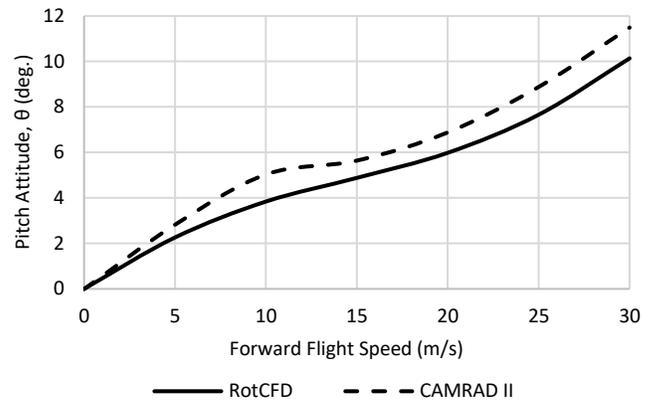Lastly, the trimmed pitch attitudes are plotted against forward flight speed in Figure 18.

Figure 18: Trimmed pitch attitude versus forward flight speed

For forward flight speeds greater than or equal to 5 m/s, RotCFD underpredicts the required pitch attitude by approximately 1 degree, on average, compared to CAMRAD II. The discrepancy could be due to a difference in airframe drag in the RotCFD and CAMRADII models or due to different rotor load dependence on pitch.

Airframe Effects on Forward Flight Results
The next set of runs sought to understand the effects of Ingenuity's airframe on the performance of the rotors in RotCFD. To do so, performance predictions are compared between the airframe-included cases and the rotors-only cases. The pitch attitudes for the rotors-only cases are set at the trimmed settings depicted in Figure 13 for forward flight speeds 5 to 30 m/s. The CAMRAD II cases are performed without the effects of the airframe.

When comparing the rotors-only cases and airframe-included cases in RotCFD, there is minimal difference seen in most performance metrics. The only metric that shows significant variation is the differential collective input, shown in Figure 19.
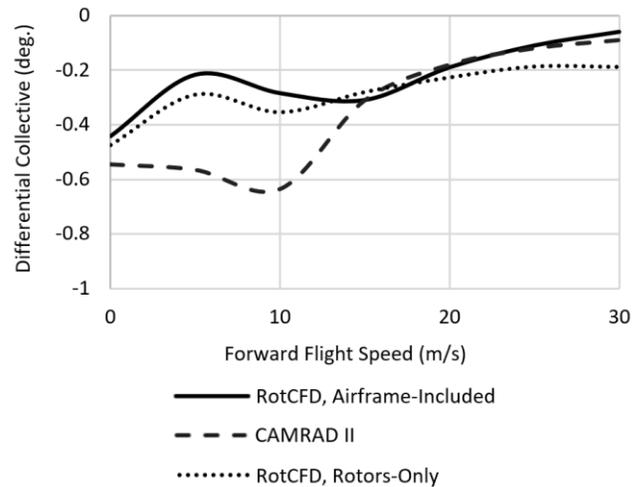

Figure 19: Trimmed differential collective settings versus forward flight speed

The differential collective setting for the RotCFD airframe-included cases requires a lesser differential at all forward flight speeds, excluding 15 m/s, where it briefly requires more than the values predicted by CAMRAD II and RotCFD without the airframe included. In contrast, there is only a marginal difference in the average collective pitch predicted for the cases in which the airframe is and is not included.

Next, the Ingenuity model is decomposed into two bodies: the main fuselage and the solar array. The cases are run again with the same conditions, and the force and moment for each individual body are recorded. The main forces of interest are the drag, or the x-component of total force, and download, the z-component of total force. These forces are divided by the dynamic pressure, to get D/q and download/q, respectively. D/q is shown in Figure 20, and download/q is in Figure 21.
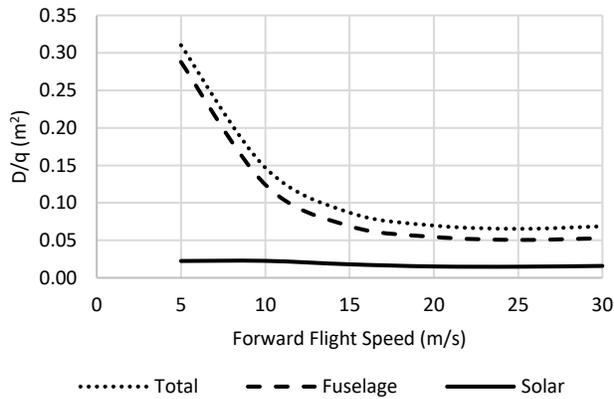

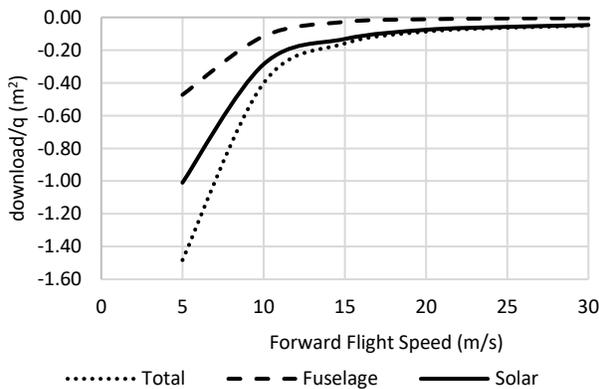**Figure 20: Drag over dynamic pressure versus forward flight speed**

Figure 21: Download over dynamic pressure versus forward flight speed

As expected, the fuselage is the main body contributing to the drag force in the results, and the solar array drives the download. The download shows that the solar array provides a small negative lifting force, especially at lower forward flight speeds. As forward flight speed increases, both coefficients approach and asymptote near zero.

It is expected that D/q should be relatively constant for a fixed frontal area and drag coefficient; this phenomenon is illustrated in Figure 20 for forward flight speeds greater than 20 m/s. Furthermore, this figure is consistent with the increase in drag coefficient observed at low Reynolds numbers [17].

The final study for airframe effects analyzes the effect pitch attitude has on drag and download. This study is conducted at a fixed forward flight speed of 20 m/s. The pitch attitude is swept from 0 to 10 deg. The solar array and fuselage remain separated to understand how different pitching angles affect the forces on each body. Figure 22 shows the D/q for this set of results, and Figure 23 shows the download/q.
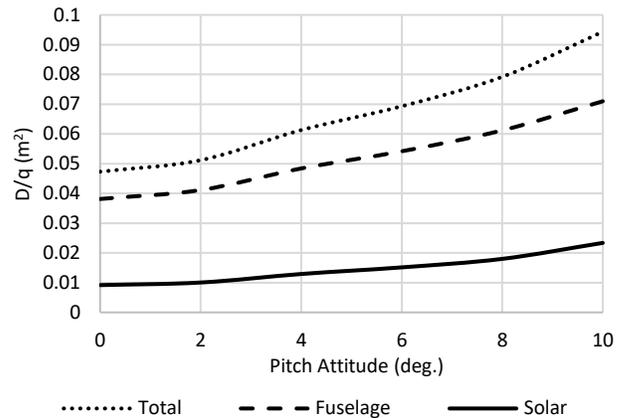

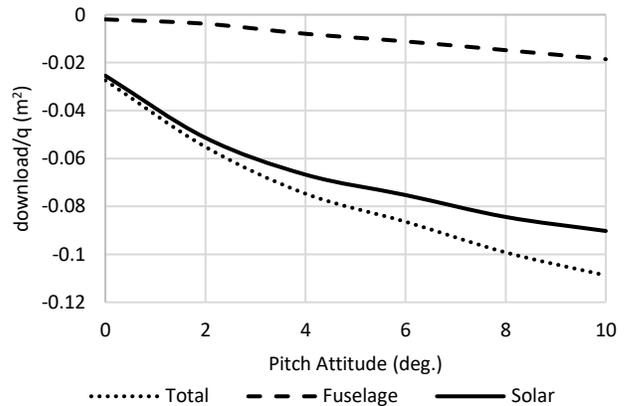**Figure 22: D/q versus pitch attitude at a forward flight speed of 20 m/s**

Figure 23: Download/q versus pitch attitude at a forward flight speed of 20 m/s

As the pitch increases, both D/q and download/q increase in magnitude, with D/q increasing positively and download/q increasing negatively. The slope of download/q versus pitch attitude indicates that more lift force is generated as the pitch attitude increases. While the trend is largely linear, at higher pitch angles, the download/q from the solar array appears to start leveling off slightly. If the solar array is considered to be a thin wing with a rectangular planform,

one could interpret this asymptotic trend to indicate that the solar array is approaching stall.

BLADE PERFORMANCE COMPARISONS

To further understand the performance predictions of Ingenuity by RotCFD and CAMRAD II, sectional blade analysis is performed. Both programs output a variety of metrics as a function of radial station, r/R, and azimuth, ψ. For this analysis, the sectional angle of attack is selected for analysis. This provides an insight into the differences in trimming behavior between the two programs.

First, the differences in sectional angle of attack between the rotors-only cases and airframe-included cases are shown. Figure 24 shows the comparison for the top rotor, and Figure 25 for the bottom rotor. Two azimuthal locations are shown on each plot, at ψ = 0 and ψ = 180 deg. Small differences can be seen between the two cases at the selected azimuthal position, mostly at lower r/R values. Nevertheless, the two cases closely agree for r/R values greater than 0.5. For low r/R values for both azimuthal locations, the local angle of attack is higher for the airframe-included cases. Likely, the presence of the airframe encumbers the induced flow near the rotors' center, thus increasing the local angle of attack.
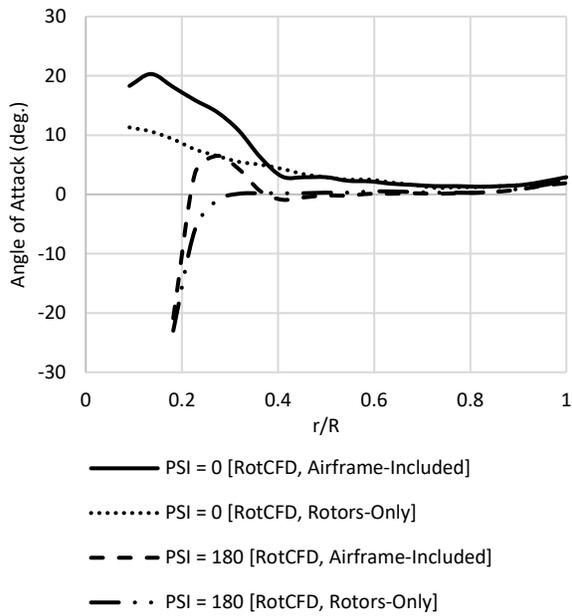

Figure 24: Sectional angle of attack versus radial station for rotors-only and airframe-included cases for the top rotor
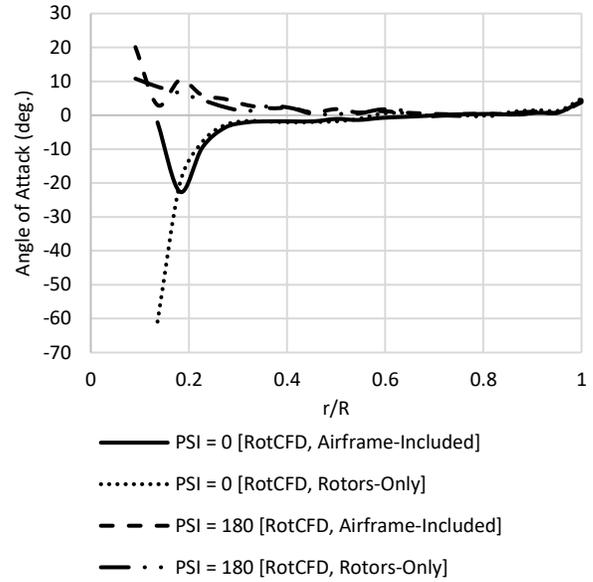

Figure 25: Sectional angle of attack versus radial station for rotors-only and airframe-included cases for the bottom rotor

Next, RotCFD and CAMRAD II are compared to each other. The rotors-only cases are selected for this comparison since there is no airframe modeled in CAMRAD II. Figure 26 shows the comparisons at two azimuthal angles for the top rotor, and Figure 27 shows the comparisons for the bottom rotor. The largest differences again occur at smaller r/R values for both rotors. For the top rotor, there is agreement for both azimuthal stations for r/R values from 0.4 to 0.7. For the bottom rotor, there is agreement at ψ = 180 deg. for r/R values from 0.4 to 0.8.
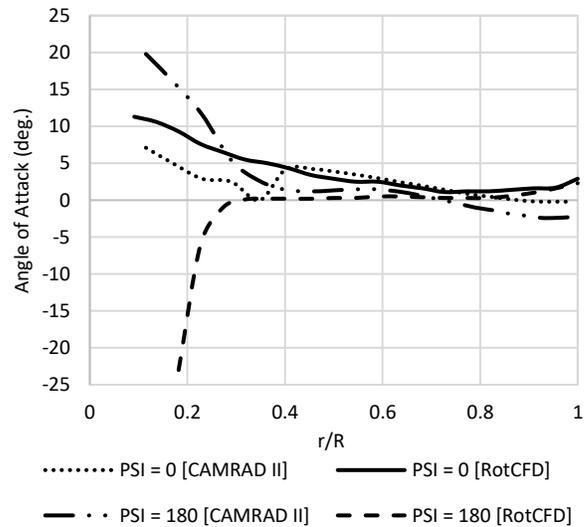

Figure 26: Sectional angle of attack versus radial station for top rotor

11

Figure 27: Sectional angle of attack for bottom rotor

One final check is to compare the sectional angle of attack as a function of azimuth angle at a fixed radial station. The location r/R = 0.64 is chosen for this comparison. Both the top and bottom rotor are shown in Figure 28. No clear trends are seen in this figure between RotCFD and CAMRAD II.

Figure 28: Sectional angle of attack versus azimuth at a fixed radial station of r/R = 0.64

The overall differences between the sectional angle of attack per radial station may provide some insight into the differences between the results from each code. However, more in-depth analysis is necessary to determine the true basis of these discrepancies.

CONCLUSION

RotCFD hover performance predictions are compared against both CAMRAD II and experimental hover test data in JPL SS conditions and solely against CAMRAD II in MC 2 conditions. For both comparisons, it is observed that all predictions are in general agreement for the design thrust coefficient range of Ingenuity. However, RotCFD predicts higher power coefficients than CAMRAD II for high thrust settings even though both codes use the same C81 airfoil tables. Disparities, therefore, also arise in comparisons of figure of merit for high collective pitch and thrust settings.

RotCFD forward flight performance predictions using rotors-only and airframe-included models of Ingenuity are compared to CAMRAD II predictions in which a rotors-only model is used. A trim surrogate model is leveraged to find pitch attitude settings in RotCFD that balance forces in the free stream direction. The trimmed settings from the surrogate are used in a comparison of trimmed forward flight simulations. The codes closely agree on the relationship between thrust and power and forward flight speed. Additionally, the trim settings are in close alignment for forward flight speeds greater than or equal to 15 m/s. Nevertheless, disparities arise in the nominal collective pitch setting and differential collective setting for low speeds. Furthermore, RotCFD underpredicts the required pitch attitude for each forward flight speed with respect to the trimmed settings of CAMRAD II.

A study of the aerodynamics of the individual components of the airframe of Ingenuity is performed. RotCFD corroborates the expected trends in how the download and drag of the solar array and fuselage vary with forward flight speed and pitch attitude. Specifically, it is confirmed that the solar array acts as a wing which generates most of the predicted download, especially for high pitch attitudes. Furthermore, it is found that the fuselage of Ingenuity generates most of the airframe drag and that the drag coefficients sharply increase for low Reynolds number flows.

Lastly, a study is conducted on the how the sectional angles of attack vary with radial station and azimuth in RotCFD and CAMRAD II. In RotCFD, it is found that the inclusion of the airframe has minimal effect on this relationship. Thus, it is reasonable to compare the rotors-only RotCFD cases with those of the CAMRAD II cases. Between RotCFD and CAMRAD II, a significant discrepancy is observed between the sectional angles of attack as a function of radial station, particularly for low values of r/R; there is agreement for r/R values between 0.4 and 0.7, generally. A similar discrepancy is observed when comparing the RotCFD and CAMRAD II predictions for sectional angle of attack versus azimuth angle.
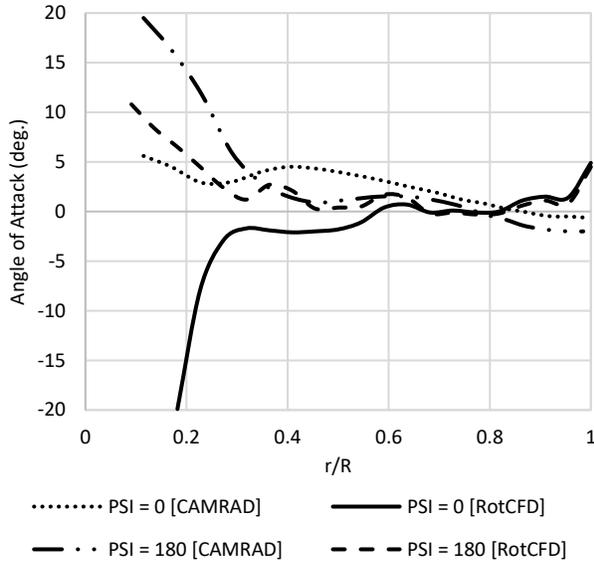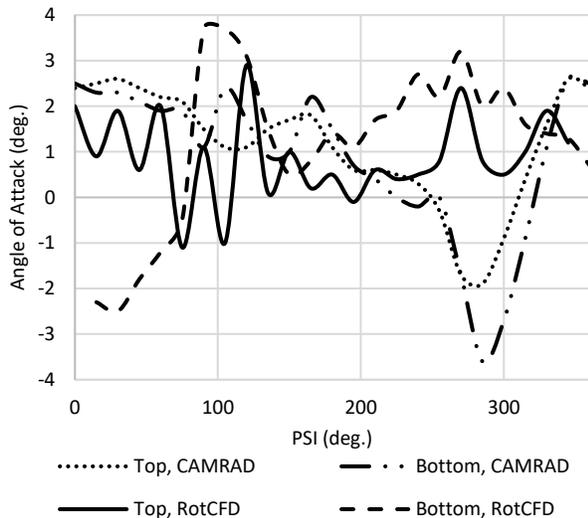
FUTURE WORK

Concerning the performance prediction comparison for hover between RotCFD, CAMRAD II, and the experimental data from JPL SS, further work is required to address the disparity in total rotor power for high collective and high thrust settings. Addressing this disparity would also address the disagreement in figure of merit predictions, as these values are coupled. Such future work includes further grid refinement studies and the analysis of rotor-disk sectional load distributions data.

Regarding forward flight results, there are several areas that require future work and attention. Firstly, additional analyses are required to understand the disparity between RotCFD and CAMRAD II in the predicted trimmed nominal collective pitch settings and trimmed differential collective settings for low forward flight speeds. Furthermore, more studies are needed to address the disagreement in trimmed pitch attitudes. To do so, it is recommended that rotors-only and airframe-only cases are simulated to distill airframe-rotor interactions and to address differences in predicted airframe drag. Once the two codes agree upon predicted airframe drag, it is anticipated that trimmed rotor settings and pitch attitudes will be in agreement for all speeds in the considered forward flight domain.

Author contacts:
Cuyler Dull: cuylerdull@gatech.edu
Lauren Wagner: lauren.n.wagner@nasa.gov
Larry Young: larry.a.young@nasa.gov
Wayne Johnson: wayne.johnson@nasa.gov

ACKNOWLEDGMENTS

REFERENCES

[1] Koning, W. J. F., Johnson, W., and Grip, H. F., "Improved Mars Helicopter Aerodynamic Rotor Model for Comprehensive Analyses," *AIAA Journal*, Vol. 57, No. 9, Sep. 2019. doi:10.2514/1.J058045

[2] Pipenberg, B. T., Keennon, M., Tyler, J., Hibbs, B., Langberg, S., Balaram, J. (B., Grip, H. F., and Pempejian, J., "Design and Fabrication of the Mars Helicopter Rotor, Airframe, and Landing Gear Systems," *AIAA SciTech 2019 Forum,* AIAA Paper 2019-0620, 2019. doi:10.2514/6.2019-0620

[3] "Ingenuity Right After a Spin," NASA Available: https://www.jpl.nasa.gov/images/ingenuity-right-after-a-spin.

[4] Balaram, B., Canham, T., Duncan, C., Grip, H. F., Johnson, W., Maki, J., Quon, A., Stern, R., and Zhu, D., "Mars Helicopter Technology Demonstrator," *2018 AIAA Atmosphere Flight Mechanics Conference,* AIAA Paper 2018-0023, Jan. 2018.

[5] Veismann, M., Dougherty, C., Rabinovitch, J., Quon, A., and Gharib, M., "Low-density multi-fan wind tunnel design and testing for the Ingenuity Mars Helicopter," *Experiment in Fluids*, vol. 62, Sep. 2021. doi:10.1007/s00348-021-03278-5

[6] Rajagopalan, R.G.; Baskaran, V.; Hollingsworth, A.; Lestari, A.; Garrick, D.; Solis, E.; and Hagerty, B. "RotCFD — A Tool for Aerodynamic Interference of Rotors: Validation and Capabilities." *American Helicopter Society Future Vertical Lift Aircraft Design Conference*, San Francisco, CA, January 2012.

[7] Mahaffy, P. R. et. al., "The Sample Analysis at Mars Investigation and Instrument Suite," *Space Science Reviews*, vol. 170, Sep. 2012, pp. 401–478. doi:10.1007/s11214-012-9879-z

[8] Koning, W. J. F., Johnson, W., and Allan, B. G., "Generation of Mars Helicopter Rotor Model for Comprehensive Analyses," *American Helicopter Society Aeromechanics Design for Transformative Vertical Flight*, San Francisco, CA, January 2018

[9] Yamauchi, G., Ed., "A Summary of NASA Rotary Wing Research: Circa 2008–2018 (Chapter 12)," NASA-TP-2019-220459, 2019.

[10] Balaram, J., and Tokumaru, P. T., "Rotorcrafts for Mars Exploration," *11th International Planetary Probe Workshop*, Pasadena, CA, 2014.

[11] Buning, P., and Nichols, R., *User's Manual for OVERFLOW 2.2*, NASA Langley Research Center, Hampton, VA, 2008.

[12] Johnson, W., "Rotorcraft Dynamics Models for a Comprehensive Analysis," *American Helicopter Society 54th Annual Forum*, May 1998.

[13] Johnson, W., "Influence of Lift Offset on Rotorcraft Performance," NASA TP-2009-215404, 2009.

[14] Harrell, J. W., and Argoud, M. J., "The 25-ft Space Simulator at the Jet Propulsion Laboratory," NASA CR 106222, Oct. 1969.

[15] Grip, H. F., Scharf, D. P., Malpica, C., Johnson, W., Mandic, M., Singh, G., and Young, L. A., "Guidance and Control for a Mars Helicopter," *2018 AIAA Guidance, Navigation, and Control Conference*, AIAA Paper 2018-1849, 2018. doi:10.2514/6.2018-1849

[16] "Mars Ingenuity Helicopter, 3D Model – NASA's Mars Exploration Program," NASA Available: https://mars.nasa.gov/resources/25043/mars-ingenuity-helicopter-3d-model/.

[17] Anderson, J. D., *Fundamentals of aerodynamics*, New York, NY: McGraw-Hill Education, 2017.